Research Article

Microwave-mediated synthesis of silver nanoparticles on various metal-alginate composites: evaluation of catalytic activity and thermal stability of the composites in solvent-free acylation reaction of amine and alcohols

Supriya[1] · Ravikant Kaspate[2] · Chandan Kumar Pal[3] · Sonali Sengupta[1] · Jayanta Kumar Basu[1]

Abstract

This work demostratres the synthesis of different metal (Ca, Zn, Ni and Cu) alginate-supported silver nanoparticles (Agnp-MA, M and A for metal and alginate respectively) by using microwave irradiation process. The characterization of these composites has been carried out through UV–vis spectra, XRD, HRTEM and FESEM analysis which confirms the formation of spherical and crystalline nanoparticles in all MA supports with particles size range of 5–8 nm. All MAs show excellent reducing and stabilizing capabilities towards Agnp and act as support for nanoparticles too. The catalytic activities of all Agnp-MAs are tested in acylation reactions of various amines and alcohols in solvent-free medium using acetic acid as green acylating agent. The detail ionic mechanism of acylation reaction has been demonstrated. Thermal stability of all catalysts was investigated through TGA analysis and the reusability of the catalysts in a reaction is explained in terms of their thermal stability. The order of stability is Agnp-CaA > Agnp-ZnA > Agnp-NiA > Agnp-CuA. Consequently, Agnp-CaA shows best reusability property than other Agnp-MAs in the reaction and can perform well up to 5th run. Heterogeneous kinetic models are proposed for the reaction.

Keywords Silver nanoparticle · Alginate · Catalyst · Thermal stability · Acylation reaction

1 Introduction

Acylation is a condensation reaction of amine and alcohol to their respective amide and organic ester. Amides and organic esters find wide applications as intermediates in versatile chemical, medical and, cosmetic industries [1]. There are several processes for the synthesis of amide and organic esters, such as using acetic anhydride or acetyl chloride as an acetylating agent in the presence of acidic and basic catalysts [2, 3]. The disadvantages of these processes are that the reagents are toxic and corrosive, and the reactions are water sensitive. Use of acetic acid instead of acetic anhydride or acetyl chloride as an acylating agent is economical as well as ecofriendly. Lewis acids such as $ZnCl_2$, $Cu(OTf)_2$, $Gd(OTf)_2$ etc. are reported to be used as catalysts for acylation reaction using acetic acid or acetic anhydride as acylating agents but with the limitation of restoring their activities till the end of the reaction which produces substantial waste [4–9]. Homogeneous catalysts inherently suffer from the disadvantage

✉ Sonali Sengupta, sonalis.iitkgp@gmail.com | [1]Department of Chemical Engineering, Indian Institute of Technology Kharagpur, Kharagpur 721302, India. [2]Department of Chemical Engineering, National Institute of Technology Srinagar, Srinagar 190006, India. [3]Department of Chemistry, Scottish Church College, University of Calcutta, Kolkata 700006, India.

of being inseparable from the product mixtures and create corrosion problem. To resolve these problems, researchers focused their attention on the synthesis of ecofriendly, inexpensive, easily recoverable, and reusable heterogeneous catalysts [10, 11]. Heterogeneous catalysts such as montmorillonite KSF or K-10 clay, HY zeolites, AgNPs@m-MgO, PANI$_n$–Fe, and mPANI/Ag are reported for acylation reaction by the use of acetic acid or acetic anhydride [2, 10–15]. One of the most important challenges in the synthesis of heterogeneous catalysts is the use of biodegradable, renewable, and inexpensive support for the active agents of the catalysts.

In the present work, silver nanoparticle on alginate is used as a catalyst in the acylation of aniline and benzyl alcohol with acetic acid. Alginate is an anionic biodegradable, renewable and inexpensive polysaccharides used as catalyst support. It is a copolymer consists of α-L-guluronate and (1−4)-linked β-D-mannuronate monomers, derived from seaweeds mainly from brown algae. A characteristic property of alginate is that it has the ability to form a hydrogel when coming in contact with metallic cations [16]. Extensive studies have been done on egg-box like structure of calcium crosslinked alginate gel when divalent calcium cation formed coordination with hydroxyl and carboxyl groups of four units of α-L-guluronate monomer from two adjacent chains of alginate polymer [17–19].

Good catalytic activity, excellent antibacterial property, high biocompatibility, ease of preparation, and low cost as compared to other noble metal nanoparticles make silver nanoparticles a preferred choice to the researchers [20–25]. Among the physical, chemical, and biological synthesis processes, microwave irradiation approach to synthesize silver nanoparticles is easier, lesser time taken and greener synthesis route. Moreover, the use of alginate as a reducing and stabilizing agent can replace hazardous ones such as sodium borohydride, hydrazine hydrate etc. [26–28].

In the current work, silver nanoparticle supported on alginate beads gelled with various divalent metal cations (Ca^{2+}, Cu^{2+}, Zn^{2+} and Ni^{2+}) were successfully synthesized using microwave irradiation and were used as catalysts in acylation of aniline and some primary and secondary alcohols, such as benzyl alcohol, ethanol, 1-hexanol, 1-butyl alcohol and 1-phenyl ethanol with acetic acid. Simple and easy separation of the prepared catalyst from the reaction medium makes it attractive for applications. The effects of different process parameters, such as catalyst loading, temperature, and different metal alginate support on the reaction, were explored. It has been of immense interest to find out the role of the various metals cross linked with alginate support on the sustainability of the catalytic activity. All the Agnp-MAs were characterized and their properties were explained in relation to the reusability of the catalyst in the reaction.

The novelty of the present work lies in the synthesis of silver nanoparticles supported on Cu-alginate (Agnp-CuA), Zn-alginate (Agnp-ZnA), and Ni-alginate (Agnp-NiA) as well as the elaboration of their stability in the reaction medium, which is a new addition to the literature. A limited number of reports are available on the preparation of silver nanoparticles supported on Ca-alginate (Agnp-CaA) [29, 30] but the application of Agnp-MA with different other metals, as a catalyst in acylation reaction of amine and alcohols with acetic acid, has not been reported yet.

2 Experimental

2.1 Materials

Sodium alginate was purchased from Loba Chemie, India. Calcium chloride, nickel (II) nitrate hexahydrate, zinc nitrate hexahydrate, copper nitrate hexahydrate, silver nitrate, aniline, acetic acid, ethanol, ethylacetate, 1-butanol, n-hexanol, 1-butyl acetate, and benzyl alcohol were procured from Merck India Ltd., India. Acetanilide,1-phenyl ethanol, 1-phenylethyl acetate, and benzyl acetate were purched from Sigma Aldrich, India. Double distilled water was used for sample preparation.

2.2 Characterization

Agnp-MAs were characterized by X ray Diffraction (XRD), UV–Vis spectra, High Resolution Transmission Electron Microscopy (HRTEM), Field Emission Scanning Electron Microscope (FESEM), Fourier-Transform Infrared Spectroscopy (FTIR), NH_3- Temperature Programmed Desorption (TPD) analysis and Thermo-Gravimetric Analysis (TGA). The analytical results are elucidated with illustrations. SHIMDZUUV 1800 UV–Vis spectrophotometer of range 200–1100 nm, are used to obtain electronic spectra. XRD is performed on X'pert^3 Powder, Panalytical, Netherlands. HRTEM and selected area electron diffraction (SAED) is conducted on HRTEM, JEM-2100F, JEOL, Japan. A slice of bead was placed on a copper grid and vacuum dried for HRTEM analysis. Thermo gravimetric analysis (TGA) is done on Thermo gravimetric analyser (Q50, TA Instruments). FESEM is performed on JSM-7610F, JEOL Japan. FTIR analysis is perform on Perkin Elmer Spectrum 100 in the spectrum range of 400–4000 cm^{-1}. NH_3-TPD analysis is performed on Chembet-3000 TPR/TPD.Gas chromatography (Perkin Elmer Clarus 480 with DB5, capillary column) was used to monitor the progress of all the reactions by reaction sample analysis and the conversion was estimated.

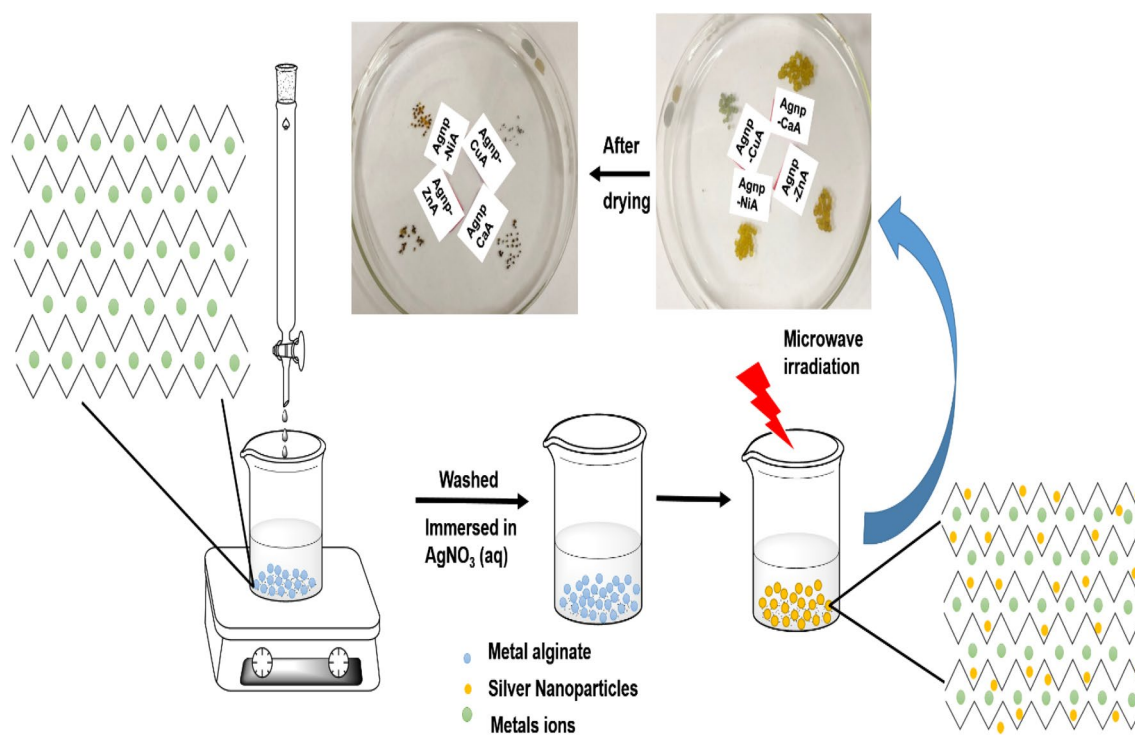## 2.3 Preparation of metal alginate-silver nanoparticles beads

It was planned to prepare a number of metal alginate beads, such as Ca, Cu, Zn, and Ni alginates and dope Ag nanoparticles to them. In the first step, an aqueous solution of Na-alginate (1.33 wt%) was added dropwise into the aqueous solutions of metal nitrate salts [Ca^{2+}, Cu^{2+}, Zn^{2+} and Ni^{2+} (0.1 M)] under stirring. As soon as the alginate drops came in contact with the metal salt solution, hydrogel beads were formed. These beads were then cured in salt solutions for a sufficient period of time of 5 h for the successful replacement of sodium ions by the metal ions. The resulting beads were then separated from the solution and washed with a copious amount of water to remove excess metal ions. This way, different metal alginate beads were formed. Impregnation of silver in the metal alginate beads was done in the next phase. The beads were soaked in silver nitrate solution for another 5 h, when adsorption of silver ion on metal alginate beads occured. This step was followed by microwave irradiation of the beads to reduce silver ion to silver nanoparticles. The microwave irradiation for 12, 15, and 20 min was done on three samples. In the final step, the beads were washed and air dried. Complete preparation stages of silver nanoparticles in different metal alginate beads and the structure of beads are shown in the schematic diagram (Scheme 1).

2.4 General procedure for acylation reaction catalysed by silver nanoparticles-metal alginate(Agnp-MA)

Acylation of aniline is done with all four Agnp-MAs to test their catalytic activity. In a typical reaction, 2 mmol aniline, 2 ml (35 mmol) acetic acid, and 150 mg Agnp-MA catalyst are taken in a closed vial and heated in an oil bath at 100 °C maintained with an accuracy of ± 1 °C for 2 h. After completion of the reaction, the catalyst was separated from the reaction mixture. Gas chromatography (Perkin Elmer Clarus 480 with DB5, capillary column) was used to monitor the progress of the reaction by reaction sample analysis and the conversion was estimated.

3 Results and discussion

Figure 1 depicts the UV–Vis spectra of different Agnp-MAs at 421, 420, 419, and 421 nm for Agnp-CuA, Agnp-CaA, Agnp-ZnA, and Agnp-NiA, respectively. These spectra confirm the formation of silver nanoparticles and hence, indicate the successful role of each alginate as reducing and stabilizing agent for Agnp formation from Ag^+ and support for them too.

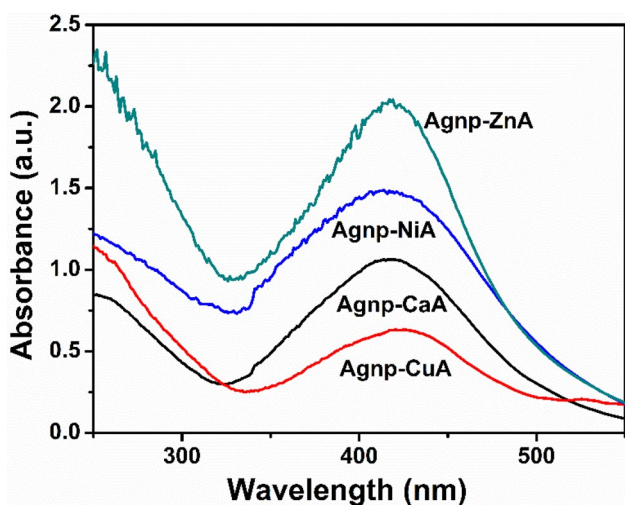**Scheme 1** Flow diagram of synthesis of metal alginate silver nanoparticles

Fig. 1 UV-Vis spectra of different Agnp-MAs

3.1 X-ray diffraction analysis

The XRD patterns of Agnp-MAs are shown in Fig. 2a–d. The diffractograms of metal alginates with and without Agnp in each figure show a typical comparison between these two types for all Agnp-MAs. XRD patterns of metal alginate without silver nanoparticles depict characteristic amorphous morphology of alginate with a broad hump at $2\theta = 20$–$50°$. The intensity of this hump is found to be lesser in CuA than that of the other three Agnp-MAs, proving more pronounced amorphous behavior of the other ones. The presence of the characteristic peak of silver nanoparticles in the diffractograms of all Agnp-MAs establishes the formation of crystalline silver nanoparticles in them. Moreover, it has been observed that the Ag peak appeared in Agnp-CuA is sharper and longer compared to that of the other three Agnp-MAs. This may be explained by the lesser amorphous character of Agnp-CuA than that of the other Agnp-MAs, which may help in revealing the sharpness of Agnp peak than for the other Agnp-MAs, where the higher amorphous behavior of MAs suppresses the actual Agnp peak. XRD pattern of Agnp-CuA represents distinctive crystalline peak of silver nanoparticles at (111), (200), (220), and (311) lattice planes of FCC silver (JCPDS: 89-3722), whereas, Agnp-CaA and Agnp-NiA attribute crystalline peaks at (111) lattice planes of FCC and Agnp-ZnA shows at (111) and (200) lattice planes of FCC.
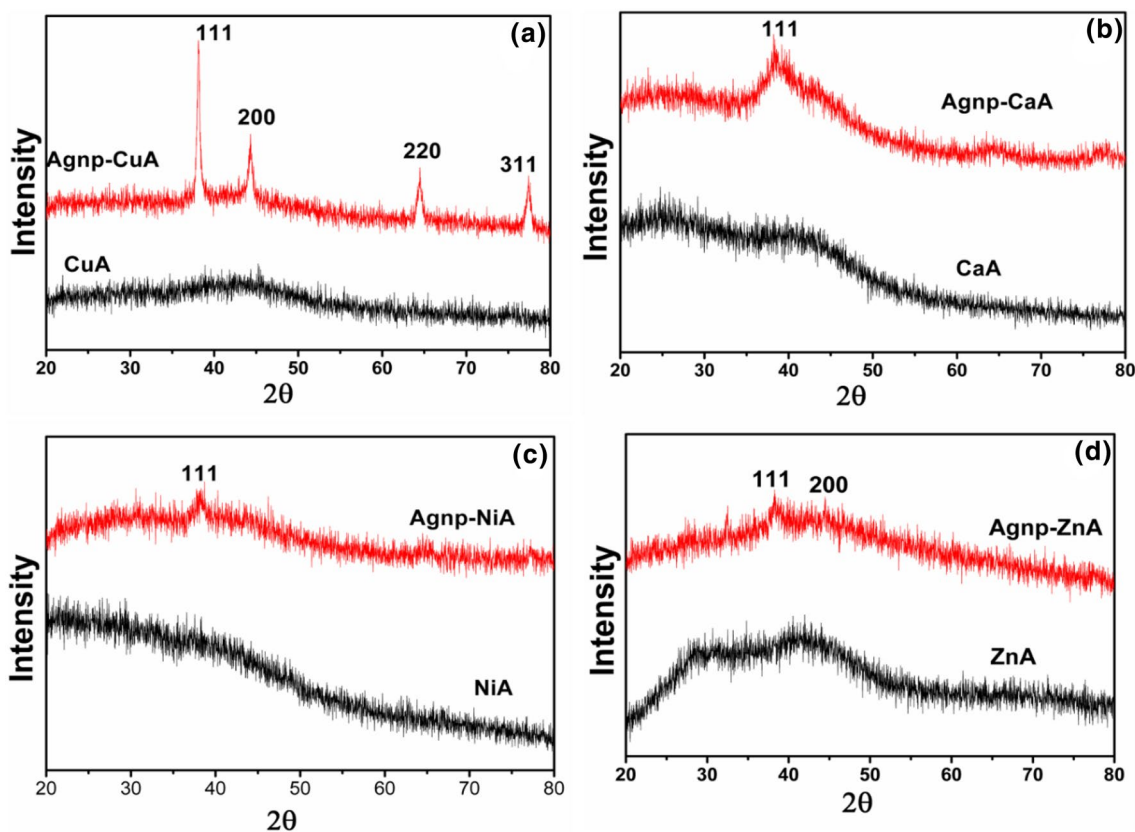

Fig. 2 XRD plots of **a** Agnp-CuA/CuA, **b** Agnp-CaA/CaA, **c** Agnp-NiA/NiA, **d** Agnp-ZnA/ZnA

3.2 Thermo gravimetric analysis (TGA) and derivative thermogravimetry (DTG) curves

TGA analysis of any sample tells about the amount of weight loss of the sample by both physical and chemical means. Physical weight loss may be associated with the loss of inherent moisture or occluded gases within the sample. Chemical weight loss is obviously related to the decomposition of the material by bond breakage and loss of lower molecular weight molecules. TGA curve is expressed by % weight loss against temperature. DTG curve can be constructed by TGA analytical data and is an expression of the rate of %weight loss against temperature.

During temperature treatment of the sample, the stage wise decomposition is expected. But many times, it is observed that the stages are overlapped with one another and may not be separately distinguished. Because of this overlapping, it is not very clear to detect a particular stage from the TGA curve only. DTG curve helps in indicating the stages of decomposition of a sample at different temperature zones by peaks or humps.

In this work, all the Agnp-MA samples are analyzed in TGA to find out their thermal stability. In this line, Fig. 3a–d depict the TGA and DTG curves of Agnp-CaA, Agnp-CuA, Agnp-NiA, and Agnp-ZnA, respectively. Table 1 describes various degradation stages with their respective temperatures for different Agnp-MAs.

For each sample, the 1st stage corresponds to physical weight loss, which is a slow process [21, 31]. After 1st stage, weight loss starts through a chemical process, which

Table 1 Detail of thermal degradation temperatures at different degradation stages

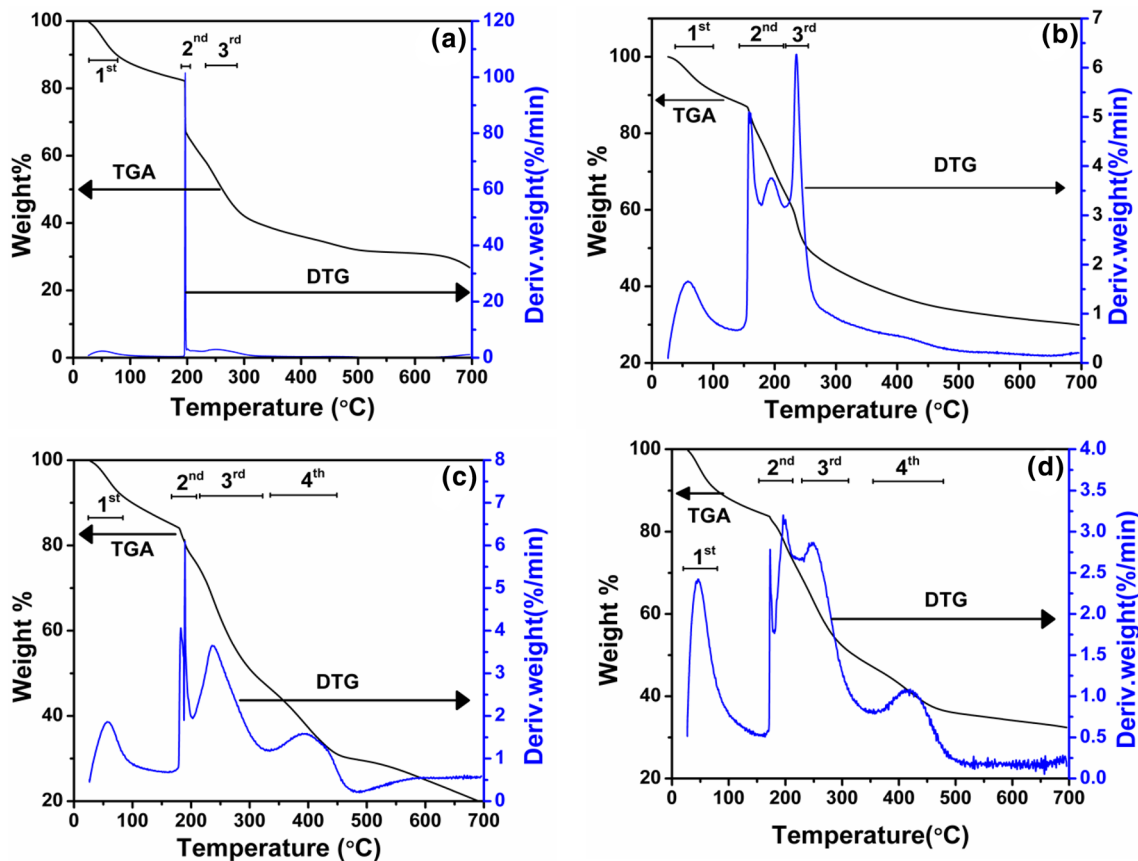| Thermal stage	1st (°C)	2nd (°C)	3rd (°C)	4th (°C)
Sample name				
Agnp-CaA	20–80	194–199	230–302	–
Agnp-CuA	20–100	145–195	216–275	–
		179–216		
Agnp-ZnA	29–100	165–178	230–304	368–495
		178–216		
Agnp-NiA	28–95	173–188	201–326	335–470
		188–201		

Fig. 3 TGA and DTG analysis of **a** Agnp-CaA, **b** Agnp-CuA, **c** Agnp-NiA, **d** Agnp-ZnA

includes different bond breaking of alginate structure. This phenomenon is mainly related to the decarbonylation, decarboxylation, and fracture of the polysaccharide polymer chain of alginate through the destruction of mainly C–H, C–O–C bonds. This decomposition stage results in the formation of CO_2, H_2O, and other lower molecular weight molecules, and this way, slowly the alginate structure breaks down as temperature increases. Different Agnp-MAs show different behavior with similar temperature treatment [31–33].

It was observed from DTG curves that, Agnp-CaA and Agnp-CuA show three stages of weight loss pattern, whereas, Agnp-ZnA and Agnp-NiA both exhibit four stages of weight loss. Another point to mention is that except Agnp-CaA, all other catalysts show two temperature ramps in 2nd degradation stage, which is clearly shown by the presence of two peaks at two different temperature ranges at that stage. The two steps degradation at the second stage may be explained by the effect of Cu, Zn and Ni ions in the degradation reaction, owing to their transition metal properties [32].

To compare the DTG and TGA curves of all samples, they are compiled together in one figure each, Fig. 4a and b respectively. In the second stage, the single degradation rate of 102%/min for Agnp-CaA is observed at degradation temperature 196 °C. At this stage, Agnp-CuA shows two degradation peaks, at 150 °C and 195 °C, with 5.07%/min and 3.76%/min rate respectively. Similarly, two peaks of Agnp-ZnA was found at 173 °C with 2.8%/min and 196 °C with 3.2%/min rates. Agnp-NiA shows the peaks at 182 °C and 188 °C with 4.08%/min and 6.105%/min rates respectively. The analytical results explain the extent of the thermal stability of different Agnp-MAs. The single degradation temperature of Agnp-CaA is high enough (196 °C) with a very high rate of degradation (102%/min) at that temperature. Other Agnp-MAs with two steps of

degradation show much lower rates. Hence, it can be clearly inferred that Agnp-CaA can withstand degradation up to a considerably high temperature, but cannot resist fast degradation after attaining that temperature. The degradation in the second stage for Agnp-ZnA starts at lower temperature (173 °C) with 2.8%/min rates than those of Agnp-NiA (182 °C with 4.08%/min rate) but later degrade more rapidly owing to the higher rate. Hence, the stability of Agnp-NiA is lesser than Agnp-ZnA. The degradation of Agnp-CuA at the second stage starts at the lowest temperature (158 °C) compared to all other Agnp-MAs. Therefore, Agnp-CuA catalyst shows the lowest stability.

In the third stage of degradation, all the Agnp-MAs undergo single step degradation. This stage is negligible for Agnp-CaA resulting in almost unnoticeable peak at 216–275 °C range. This peak is prominent for others, with Agnp-CuA at 230–320 °C, Agnp-ZnA at 230–304 °C and Agnp-NiA at 201–326 °C. Degradation of all Agnp-MAs at different temperatures correspond to different rate of degradation.

The second and third stages are interrelated. Decarbonylation, decarboxylation, and destruction of the polymeric chain of alginate through destruction of C–H and C–O–C bond, breakage of Agnp-alginate bond, and releasing of CO_2, H_2O and other lower molecular weight molecules start from the second stage, slowly progress and complete at the end of third stage [33–35].

3.3 HRTEM and FESEM Analysis

Figure 5a–d represent SAED patterns of HRTEM images of all Agnp-MA beads. The crystalline nature of Agnp can also be represented by selected area electron diffraction (SAED) other than XRD. The characteristic peak of Agnp is not properly distinguished in XRD of Agnp-MAs. Being amorphous in nature, alginate might have influenced the
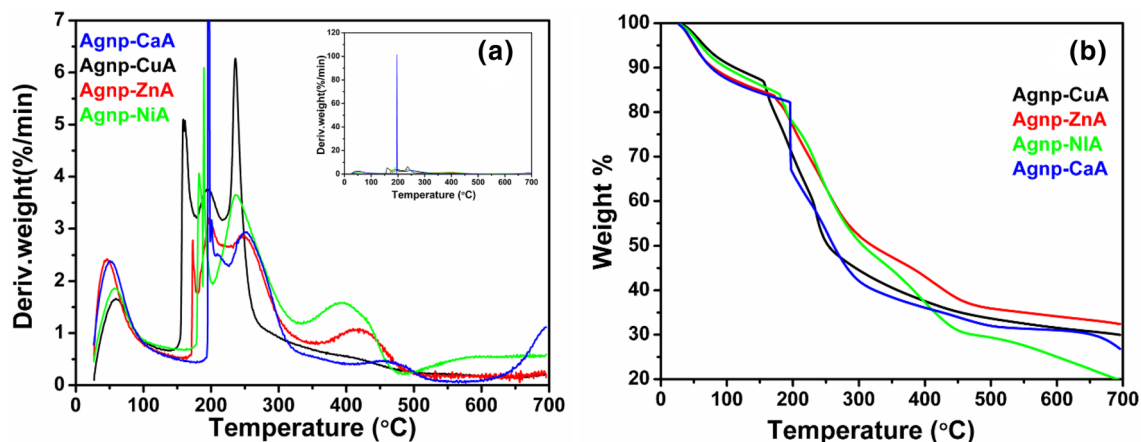

Fig. 4 **a** Zoom form of main DTG curve (inset contain main curve), **b** TGA curve for all sample
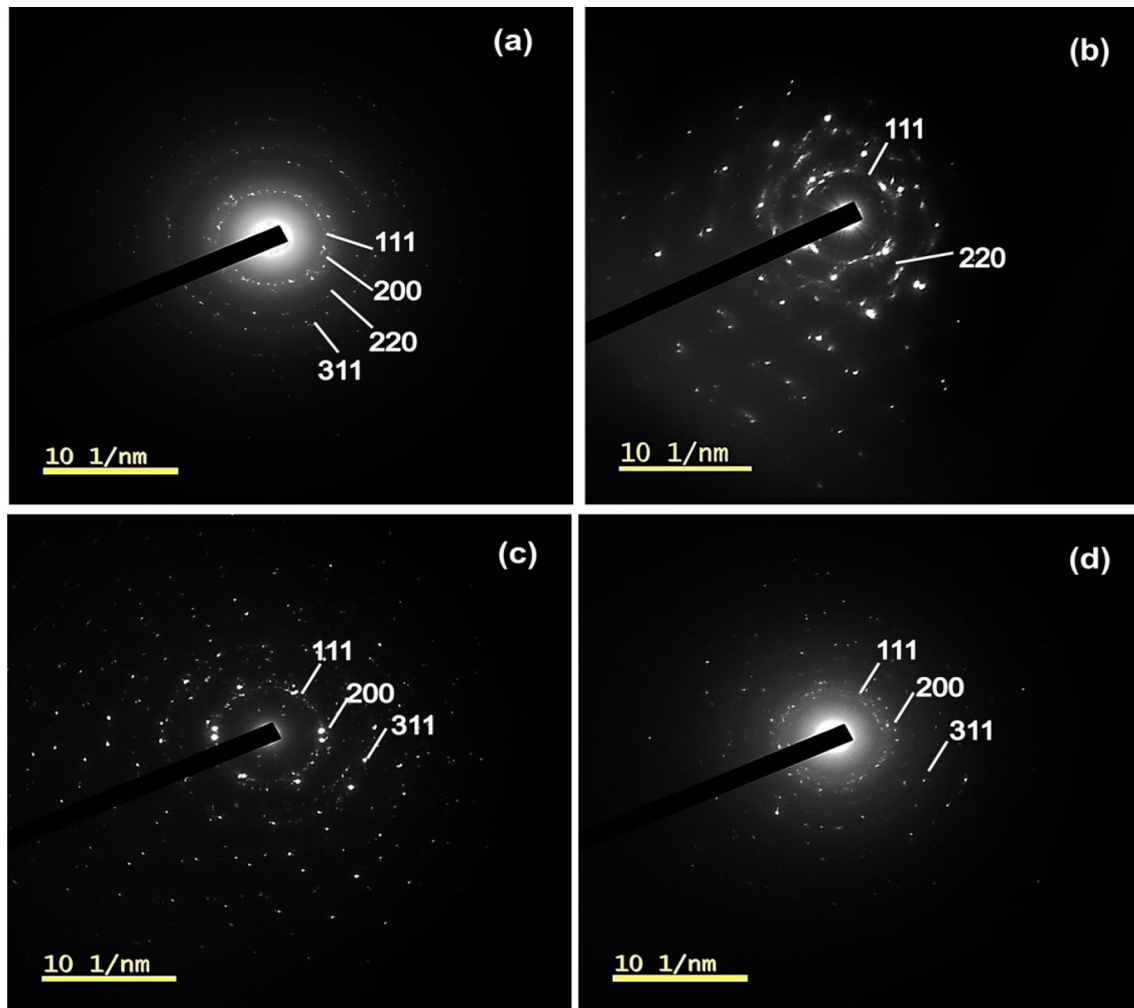
Fig. 5 SAED pattern of HRTEM image of **a** Agnp-CaA, **b** Agnp-CuA, **c** Agnp-NiA, **d** Agnp-ZnA

crystalline behavior of Agnp formed in it, and hence, XRD patterns of Agnp-MA do not show prominent and sharp Agnp peak. Agnp-CuA has lesser influence, unlike others, and Agnp peak is clearly found in it. SAED pattern confirms the formation of polycrystalline Agnp. SAED pattern of Agnp-CuA is found unable to show all the crystalline phases, as is shown in XRD. The reason may be the low thermal stability of Agnp-CuA beads at a high voltage of the beam used in HRTEM. HRTEM images of Agnp-CaA and Agnp-NiA are shown in Fig. 6a, b. The images confirm the formation of spherical nanoparticles with uniform distribution.

Figure 7a–d represent SE micrographs of all Agnp-MAs, and the inset of each image contains a histogram of Ag particles distribution in the matrix. Average particle sizes are found to be 7.56 ± 1.84 nm, 5.65 ± 1.5 nm, 5.7 ± 1.5 nm, and 5.84 ± 2 nm for Agnp-CuA, Agnp-ZnA, Agnp-CaA, and Agnp-NiA respectively. Agnp in CuA is found to be larger in size, whereas the sizes of Agnp in other MAs are more or

less the same. Narrow nanoparticle size distribution for all Agnp-MAs is observed from standard deviation.

3.4 Fourier-transform infrared spectroscopy analysis

FTIR results of all metal alginate beads with and without Agnp are shown in Fig. 8 and their peak details are given in Table S1 of supplementary file. FTIR spectra of all Agnp-MA beads at 3436 cm^{-1} and 3437 cm^{-1} represent the stretching vibration of O–H bonds where, similar bonds are also found in all MA beads (without AgNP) in the range of 3436–3449 cm^{-1} [36, 37]. The spectral peaks at (2853, 2854) cm^{-1} and (2924, 2925) cm^{-1} correspond to symmetric and asymmetric vibration of C–H starching respectively in all alginate beads with and without Agnp [37].The strong spectral band at (1631–1636) cm^{-1} are attributed to asymmetric stretching vibration of C=O of carboxylic group, although theoretically this band should appear at

Fig. 6 HRTEM images of **a** Agnp-CaA, **b** Agnp-NiA
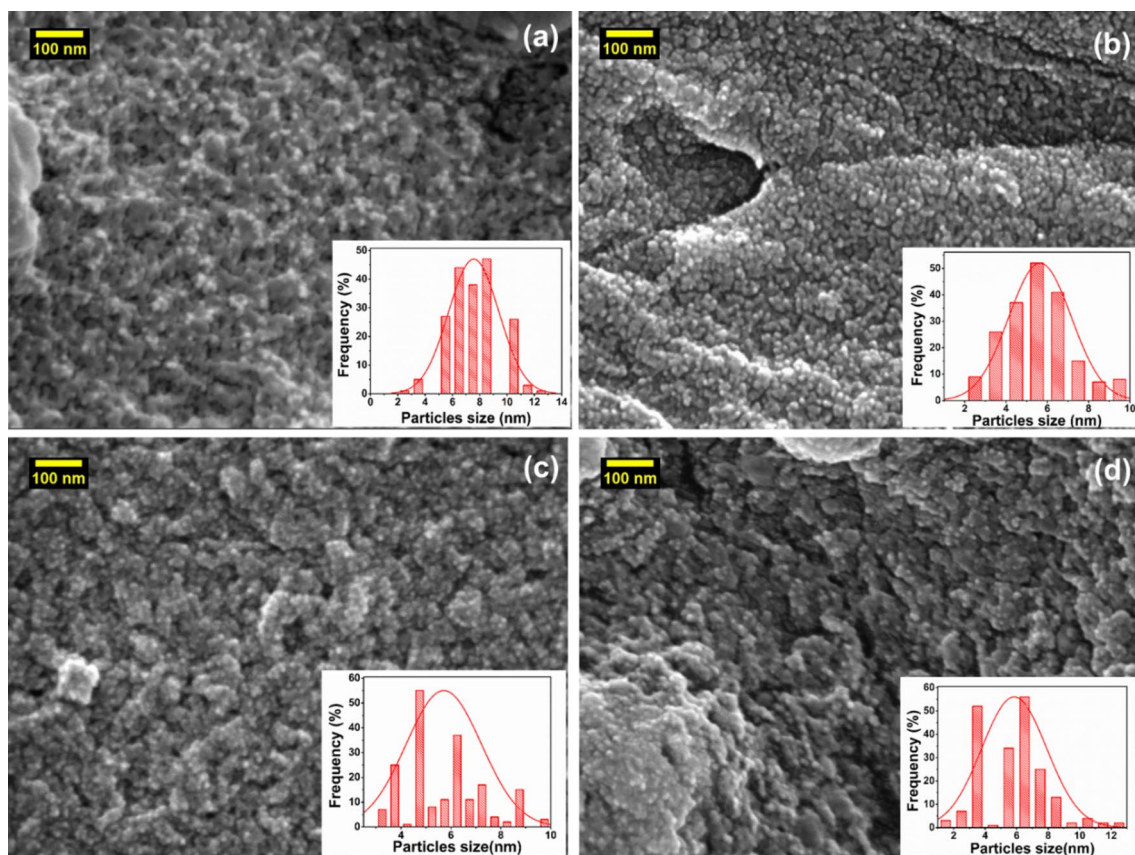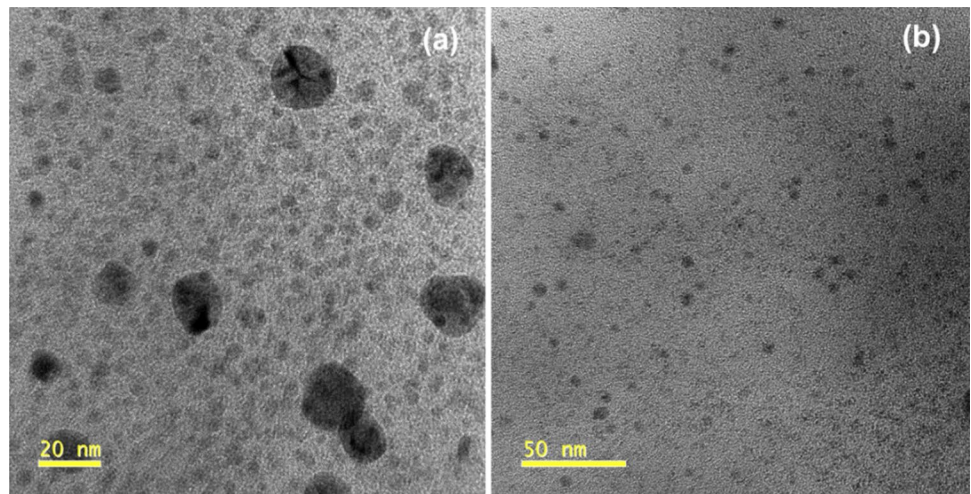
Fig. 7 SEM images of **a** Agnp-CuA, **b** Agnp-ZnA, **c** Agnp-CaA, **d** Agnp-NiA

$1709\ cm^{-1}$, this splitting of one band into two indicates the presence of intermolecular hydrogen bridge [36]. The band at the range of $1413–1438\ cm^{-1}$ may be attributed to symmetric stretch of carboxylate group in all metal alginate beads, with and without Agnp [36, 37]. Moreover, these peaks may appear due to the aliphatic (CH_2 and CH_3) angular bending modes. Two new peaks, at 1385

and $1316\ cm^{-1}$ ranges are observed in all Agnp-MA beads which may be due to the oxidation of >CHOH to >C=O in the process of reduction of Ag^+ to $Ag°$, which was found during synthesis of Au and Ag nanoparticles in alginate as reported in literature [29, 38]. The peak at $1385\ cm^{-1}$ may be attributed to symmetric stretch of carboxylate group and $1315–1316\ cm^{-1}$ correspond to C–O stretching
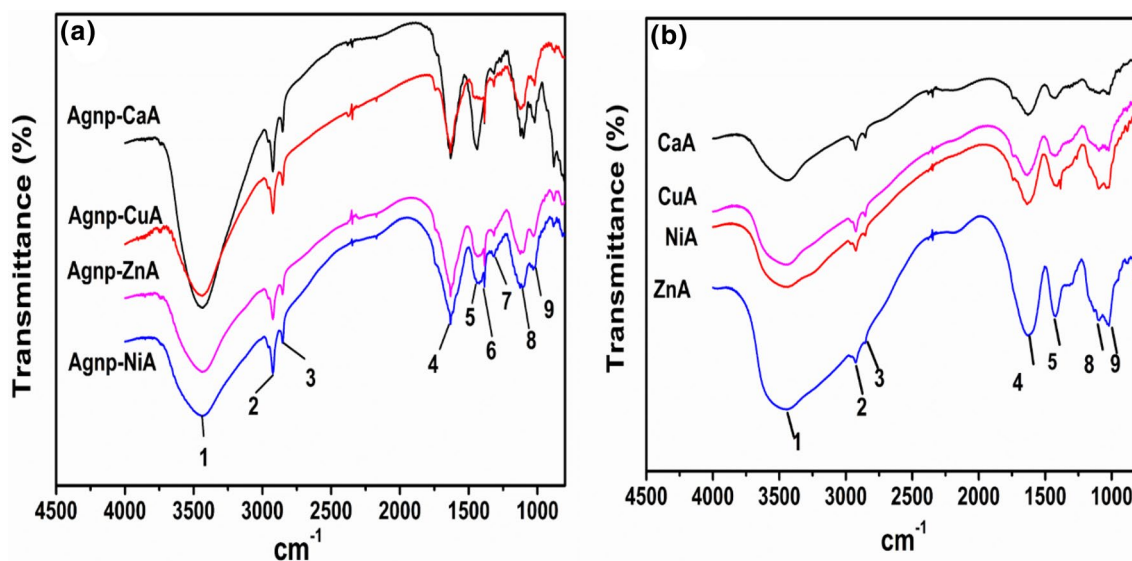
Fig. 8 FTIR results of all metal alginate beads with and without Agnp

vibration of carboxyl group. The peak at 1123–1126 cm^{-1} represents C–O stretching vibration of ester group [37]. The spectral peak at the range of 1020–1031 cm^{-1} appears because of stretching vibration of the C–O bond of glycosidic linkage between β-D-mannuronic and R-L-guluronic acid and is an indication of the degree of stability of the linear chain in the alginate [37–40].

3.5 NH$_3$—temperature programmed desorption analysis

The acidity of catalysts and total acidic sites are evaluated by NH$_3$-TPD analysis. Various temperatures of NH$_3$ desorption predict the weak, medium, and strong acid sites. The temperatures 150–300 °C, 300–500 °C and ≥ 500 °C represent weak, medium, and strong acid sites, respectively [41]. The total acidity of the catalyst was measured by summing all the actives sites concentrations. Figure 9 depicts peaks obtained from NH$_3$-TPD analysis of all Agnp-MAs. It is observed that, Agnp-CaA and Agnp-ZnA show all three acid sites which are clear from their peaks. Agnp-NiA shows medium acid sites and Agnp-CuA shows weak acid sites. The total acidity of all Agnp-MA catalysts is tabulated in supplementary file Table S2. Agnp-ZnA is found to show the highest acidity (98 mmol/g) followed by Agnp-CaA (90 mmol/g). Higher acidity may represent the proper distribution of acid sites [42]. Moreover, it is observed from the table that, although Agnp-CuA shows higher total acidity than Agnp-NiA, yet the former is found to have only weak acid sites and later has medium acid sites. Due to the higher acidity of Agnp-CaA and Agnp-ZnA
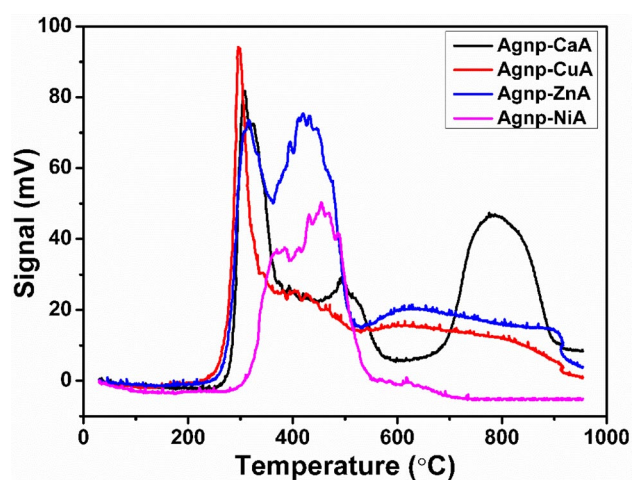

Fig. 9 NH$_3$-TPD profiles of all Agnp-MA beads

than the others, these catalysts perform better with higher conversion in the reaction than the other two.

3.6 Catalytic activity

Acylation of aniline with acetic acid as an acylating agent to produce acetanilide in solvent free condition using Agnp-MA catalysts was chosen as a model reaction to test their catalytic activity. Scheme S3 in supplementary file describes the reaction. The reaction was tested with the catalysts prepared at three different microwave (MW) irradiation times, 12, 15, and 20 min. The conversions with all these catalysts are tabulated in Fig. 10. The conversions with catalysts prepared with 15 min irradiation time are
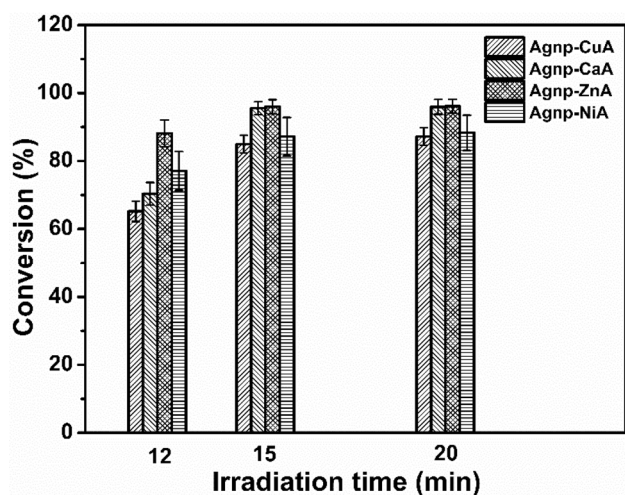
Fig. 10 Effect of Agnp-MA catalysts prepared at different MW irradiation times on conversion of aniline in acylation reaction (Aniline: 2 mmol, acetic acid: 2 ml, catalyst: 150 mg, Temperature: 100 °C, Time: 2 h.)

found more than that with the catalysts prepared with 12 min MW time, but the catalysts prepared with 20 min irradiation time fail to improve the conversion any more from those with 15 min irradiation time. This stands proof of lesser production of Agnp from silver ion in 12 min irradiation than that with the other two, and 15 min irradiation time is the optimum time of irradiation to produce maximum Agnp. Therefore, all subsequent reactions were conducted with catalysts produced by MW irradiation of 15 min. Among all the Agnp-MA beads, Agnp-ZnA, and Agnp-CaA produce 96% conversion, which is higher compared to the conversion with Agnp-CuA(87%) and Agnp-NiA (88%) at the same conditions of 2 h at 100 °C with equal amount of catalysts. Here it proves the role of higher acidity of the two former catalysts than the latter two. Reaction was also conducted in the absence of the catalyst, and 40% conversion was achieved as shown in Table 2. Effect of different metal alginates (CuA, CaA, ZnA and NiA) as support on acylation reaction was also tested by carrying out the reaction with them only. As shown in Table 2, conversions of aniline with different metal alginates are almost the same (42–44%) as that without catalyst (40%). This result indicates that alginate support has no contribution to the acylation of aniline. This result also confirms

Table 2 Effect of different metal alginates on acylation of aniline[a]

Catalyst	No catalyst	CuA	CaA	ZnA	NiA
Conversion (%)	40	42	44	44	41

[a]Aniline: 2 mmol, acetic acid: 2 ml, catalyst: 150 mg, Temperature: 100 °C, Time: 2 h

that adsorption of the reactant aniline does not take place on the alginate surface for further progress towards reaction. Hence, it can be clearly said that alginate cannot provide any catalytic active site and Agnp embedded on them act as the necessary active sites for the reaction to happen on Agnp-MAs.

The effect of the amount of Agnp-ZnA catalyst varying from 50 to 200 mg (12–48 μmol Agnp) on the reaction is shown in Fig. 11. The conversion is found to increase from 50 to 150 mg of catalyst and further increase in catalyst loading does not produce any better conversion rather remains almost the same. This indicates that 150 mg of catalyst weight (35.84 μmol Agnp) is the optimum amount for the reaction, and probably the maximum conversion obtained is the equilibrium conversion.

The effect of temperature on the conversion of aniline is shown in Fig. 12 varying the temperature in the range of 70–100 °C with the conversion of aniline from 44 to 96%. This result indicates that the reaction is favoured at higher temperature. Reaction with temperature beyond 100 °C was not performed as at higher temperature; the degradation of catalysts may start as experienced from TGA analysis. Hence, 100 °C is chosen as operating or optimum temperature for the subsequent reactions.

Activation energies of acylation reaction of aniline with acetic acid were determined by Arrhenius plot with and without catalyst Agnp-CaA and the plots are shown in Fig. 13a and b respectively. The activation energies are calculated to be 55.79 and 102.14 kJ/mol with and without catalyst respectively. The values of activation energies prove the advantage of using catalyst in the reaction which results in bringing down the activation energy to
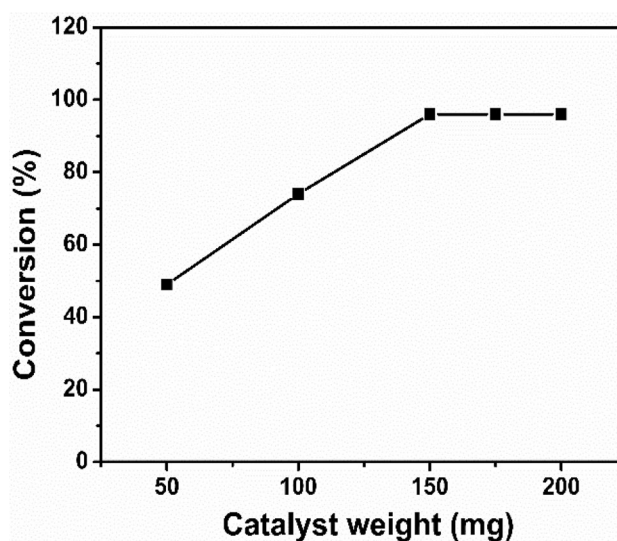

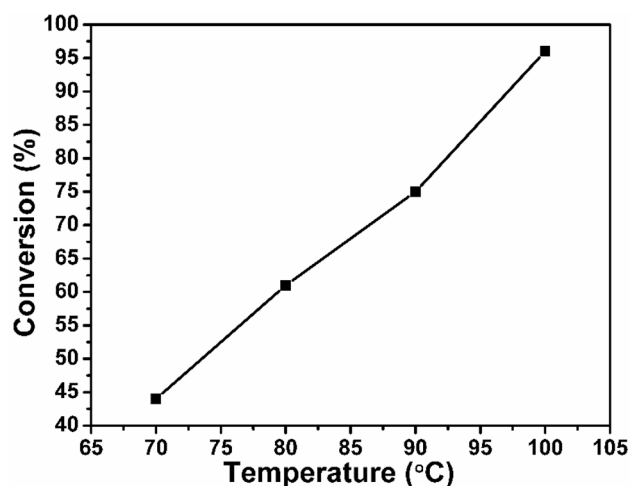**Fig. 11** Effect of catalyst amount for acylation of aniline (2 mmol) with acetic acid (2 ml) at 100 °C

Fig. 12 Effect of temperature on acylation of aniline (2 mmol) with acetic acid (2 ml)

Table 3 Effect of different metal alginate catalysts on conversion of benzyl alcohol in acylation reaction[a]

Catalyst	No cata-lyst	Agnp-CuA	Agnp-CaA	Agnp-ZnA	Agnp-NiA
Conver-sion (%)	< 5	82	91	90	83

[a]Benzyl alcohol: 2 mmol, acetic acid: 2 ml, catalyst: 150 mg, Temperature: 100 °C, Time: 4 h

almost half from that of the reaction carried out without catalyst. Calculation of apparent rate constant (k_{app}) is given in supplementary document.

3.7 Catalytic acylation of benzyl alcohol with acetic acid

Acylation of benzyl alcohol with acetic acid for the production of benzyl acetate in solvent free condition was chosen as another model reaction for testing the catalytic activities of all Agnp-MAs. The reaction is shown in Scheme S4 of supplementary file. The reaction shows less than 5% conversion in the absence of the catalyst. The conversions with all Agnp-MAs as catalysts are tabulated in Table 3. Here again, Agnp-CaA with 91% and Agnp-ZnA with 90% conversion perform better than Agnp-CuA and Agnp-NiA with 81 and 83% conversions respectively.

We have seen that free alginic acid has no catalytic activity, neither calcium alginate acts as a catalyst, it is only the silver(0) embedded in bivalent metal alginate matrix which is the effective catalyst with variation in the catalytic activity and that depends on the nature of the bivalent cation. The reduction of silver (I) to nanosilver(0) in one pot synthesis effects in oxidation of the vicinal dihydroxy group on the alginic acid framework to α-hydroxy ketone on alginate polymer matrix in which the silver(0) remains embedded. It is this α-hydroxy ketone on alginate moiety which plays a key role in the acyl cation generation. It is quite justified that free alginic acid or bivalent metal alginate being devoid of this α-hydroxy ketone group fails to catalyze the acylation.

It is observed that catalytic efficiency is highest with M = Ca(II) and is slightly less for M = Zn(II); however, somewhat less efficiency is observed with Ni(II) and Cu(II). Both Ca(II) and Zn(II) are redox-innocent metals hence aptly fit with the criterion of acylation, a conventional acid–base type of reaction. The observed slightly lower efficiency of Ag(0)/Zn(II)-A is not unexpected for Zn(II) being a transition metal ion with closed valence d-subshell, that imparts higher effective nuclear charge imparting a drop in ionic radius compared to Ca(II)effecting greater covalent character. This probably retards anchoring of the substrate on the
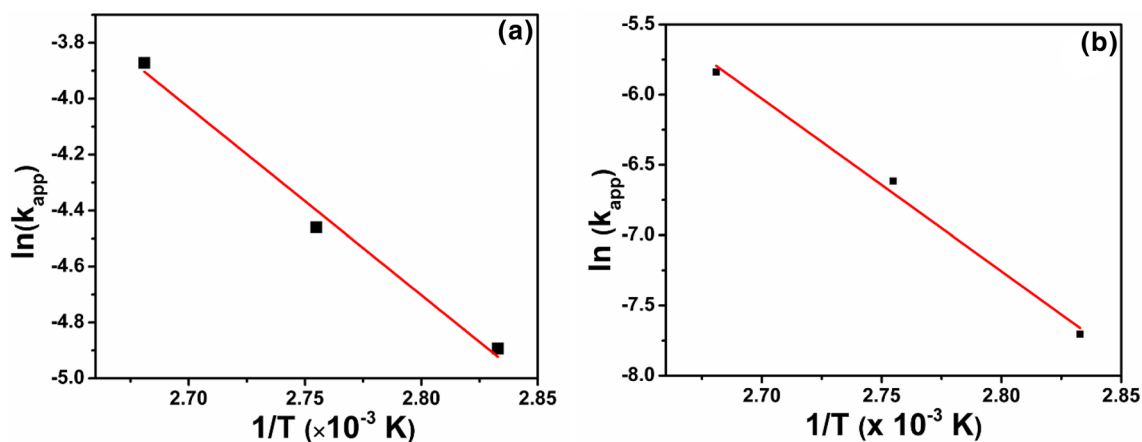

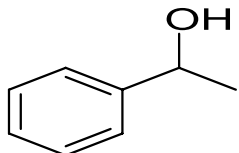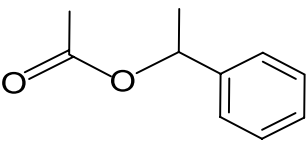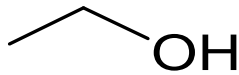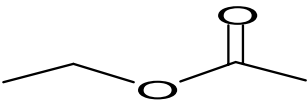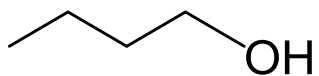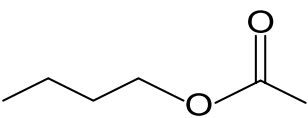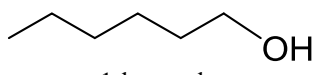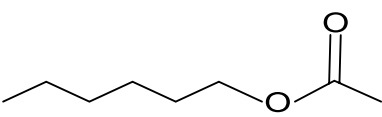**Fig. 13** Arrhenius plot **a** with catalyst, **b** without catalyst

alginate matrix, which initiates the catalytic reaction. The lower efficiency of the other two metal alginates could be understood from their redox-active character, with imminent Cu(I)/Cu(II), Ni(II)/Ni(III) changes which might perturb the catalytic activity. The shorter ionic radii of these ions also impart considerable covalent character around the alginate polymer matrix, which ultimately weakens the adherence of the electrophile generator substrate that triggers the catalytic action.

Several other acylation reactions of some primary and secondary alcohols, such as ethanol, 1-butyl alcohol, 1-hexanol and 1-phenyl ethanol with acetic acid, have been carried out with Agnp-CaA catalyst to find the influence of molecular structures of different alcohols on the reaction. It is observed that secondary alcohol1-phenyl ethanol (entry 1 of Table 4) produces 64% conversion in 4 h of reaction whereas, benzyl alcohol, a primary alcohol, shows 91% conversion at the same reaction condition [13].Another important observation is that long chain alcohol performs better than short chain alcohol in the same homologous series, which is shown in entry 2–4 of the table. This may be the consequence of electrophilic nature of alcohol [10, 13, 43], the intermediate product is more stable in long chain compared to shorter chain.
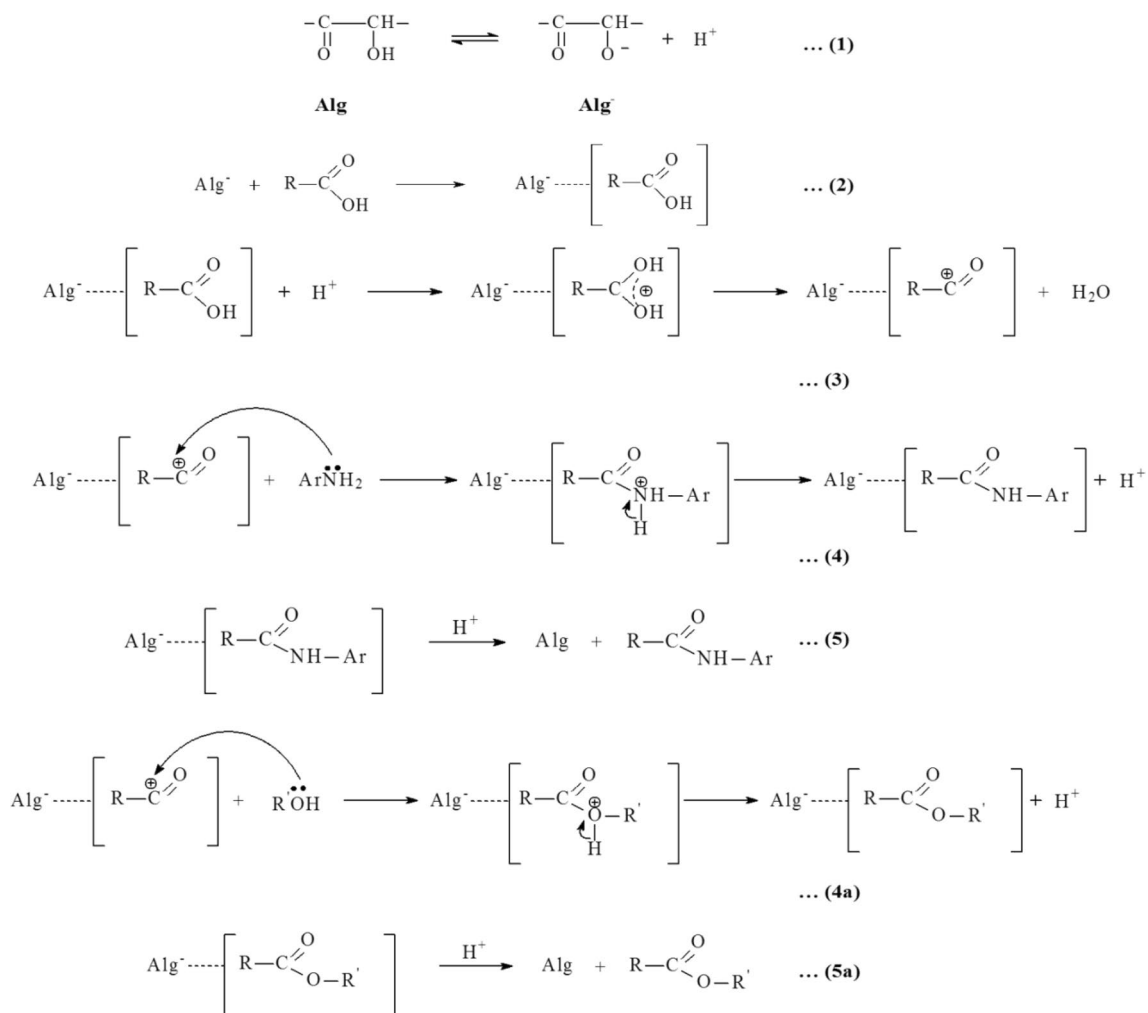
3.8 Mechanism of acylation of amine and alcohol with acetic acid using Agnp-MA catalyst

The mechanism of acylation reaction with Agnp-MA catalyst for amine and alcohol is shown in Scheme 2. The Ag(0)-M(II)alginate, represented as [Ag°/M-Alg] gel contains an oxidized α-hydroxy ketone on alginate polymer matrix with embedded nano-silver(0). The hydroxy group adjacent to a ketonic moiety on the alginic acid is a weak acid and undergoes dissociation to release proton in the medium and it becomes anionic depicted as Alg⁻ in step (1). The anionic Alg⁻ then draws the substrate acid, which gets anchored on it [step 2]. The anchored acid generates the acyl cation in step (3). The generation of acyl cation is crucial and this weak electrophile is the potential centre for the subsequent nucleophilic attack by the amino substrate in step (4) and alcoholic substrate in step 4(a); both these release proton in the process. The final step (5) in case of amine and step (5a) in case of alcohol, utilizes this proton to regenerate the Alg and the acylated product.

Table 4 Acylation of different alcohols with acetic acid using Agnp-CaA[a]

Si. no.	Reactant	Product	Conversion (%)
1	1-phenyl ethanol	1-phenylethyl acetate	64
2	Ethanol	Ethyl acetate	68
3	1-butyl alcohol	1-butyl acetate	77
4	1-hexanol	1-Hexyl acetate	89

[a]Substrate: 2 mmol, acetic acid: 2 ml, catalyst: 150 mg, Temperature: 100 °C, Time: 4 h

Scheme 2 Mechanism of acylation reaction of amine and alcohol with Agnp-MA as catalyst

3.9 Heterogeneous kinetic studies

Acylation of benzyl alcohol with acetic acid may be explained by either Langmuir- Hinshelwood (L–H) or Eley–Rideal (E–R) kinetics and the actual rate model can be determined by comparing the rate parameter values of both the kinetic models. Heterogeneous rate expression is given in the Eq. (1). The experimental data are fitted in both the L–H dual site (Eq. 2) and E–R single site (Eq. 3) models with the irreversible surface reaction as the rate controlling step. The values of the model-fitting parameters for both L–H and E–R models are estimated by using Polymath 6.0 software and are tabulated in Table 5. There is a small difference in adjusted R^2 values of L–H and E–R model. L–H model is fitted well in the reaction.

Overall rate of reaction can be stated as,

Table 5 L–H and E–R model fitting parameters

Model	Variable	Value	95% confidence	R^2	R^2 adj
L–H model	k	0.354	0.0006	0.985	0.97
	K_A (l/mol)	2.232	0.014		
	K_B (l/mol)	0.224	0.0005		
	K_C (l/mol)	10.75	0.025		
E–R model	k	0.025	4.89E−05	0.979	0.968
	K_A (l/mol)	2.245	0.019		
	K_C (l/mol)	11.1	0.036		

$$-r_A = \frac{1}{W}\frac{dC_A}{dt} \qquad (1)$$

where r_A rate of the reaction (mol/g min), W weight of the catalyst (mg/l), C_A concentration of aniline (mM), t time (min).

The rate law considering Langmuir–Hinshelwood mechanism is expressed as,

$$r = \frac{kC_A C_B}{\left(1 + K_A C_A + K_B C_B + K_C C_C\right)^2} \tag{2}$$

The expression of rate according to Eley–Rideal (assuming that only aniline adsorbs on the catalyst surface) is stated as,

$$r = \frac{kC_A C_B}{\left(1 + K_A C_A + K_C C_C\right)} \tag{3}$$

where C_A, C_B and C_C are concentrations of aniline, acetic acid and product (acetanilide) respectively and k is constant obtained from combined rate parameters. K_A, K_B and K_C are adsorption equilibrium constants of aniline, acetic acid and product (acetanilide) respectively.

3.10 Thermodynamic parameter analysis

Thermodynamic parameters of a reaction are determined using the Eyring equation (Eq. A), and the plots of $1/T$ versus $\ln(k_{app}/T)$ are shown in Fig. 14. Change in entropy and enthalpy has been calculated from the intercept and slope of the plot. Change in enthalpy of reaction is found to be $+52.77$ kJ/mol K. Positive value of enthalpy represents that reaction is exothermic in nature. Change in entropy of reaction is calculated as -0.131 kJ/K.

$$\ln \frac{k_{app}}{T} = \ln \frac{k_B}{h} + \frac{\Delta S}{R} - \frac{\Delta H}{R}\frac{1}{T} \tag{A}$$

where, k_B is Boltzmann constant (1.381×10^{-23} J K^{-1}) and h is Planck constant (6.626×10^{-34} J s).
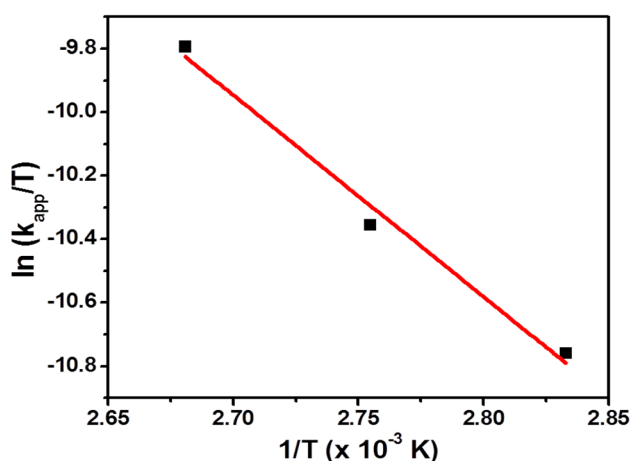

Fig. 14 Plot of $1/T$ vs $\ln(k_{app}/T)$

3.11 Reusability of catalysts

Reusability of all Agnp-MA catalysts were tested in acylation reaction of aniline with acetic acid and the results are shown in Fig. 15. After each run, the catalyst was washed with acetone and dried in vacuum for further use. It is observed from the figure that Agnp-CaA and Agnp-ZnA show reusability performance with good efficiency up to 5th run, but Agnp-CuA and Agnp-NiA cannot perform that good. Agnp-CuA could sustain up to 3rd stage of reuse and Agnp-NiA could go upto 4th stage, although with lesser conversion compared to the former two Agnp-MAs. It is practically observed during experimental runs that Agnp-CuA was completely dissolved in the reaction medium at the end of the 3rd run. This behavior of the catalyst can be explained by low thermal stability, as observed from TGA results. The analytical results show that the degradation of Agnp-CuA starts at the lowest temperature (145 °C) compared to other Agnp-MAs. Therefore, Agnp-CuA catalyst possesses lowest stability. Not only the temperature, but the repeated use of the catalyst at lower temperatures is also responsible for the onset of degradation. The thermal stability of Agnp-NiA is found to be somewhat better than that of Agnp-CuA. Because of this, degradation of Agnp-NiA catalyst started later, and it can withstand the use of it up to 4th run, after which some beads get disintegrated and hence are not in a position to use further. The degradation of Agnp-ZnA is observed to start from 4th run but can hold its activity till 5th run. After 5th run, this catalyst was not in the form or condition for next use. The highest thermal stability for Agnp-CaA among all Agnp-MAs was observed from TG analysis, and this result was reflected in the result of the reusability of this catalyst. Agnp-CaA
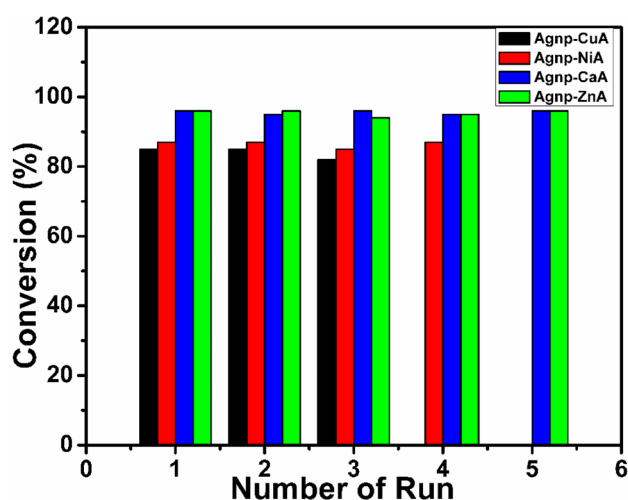

Fig. 15 Reusability of Cu-Agnp (black), Ni-Agnp (red), Ca-Agnp (blue) and Zn-Agnp (green) catalysts on acylation reaction of aniline

catalyst is found to remain in the reaction mixture up to 5th run without much change.

4 Conclusion

A simple and environment-friendly process was used for the synthesis of different metal alginate supported silver nanoparticles, and these composites are used as catalysts for acylation of aniline and benzyl alcohol using acetic acid as a green solvent. SEM, XRD and HRTEM analysis confirm the formation of spherical nanoparticles within the size range of 5–8 nm with crystalline FCC structure. TGA and DTG analysis of all Agnp-MAs show that Agnp-CuA is least stable and Agnp-CaA is the highest stable composites. All the catalyst shows good conversion in the acylation of aniline and benzyl alcohol using acetic acid. Reusability of catalyst depends on the thermal stability of the catalysts and Agnp-CaA and Agnp-ZnA show thermally stable up to 5th and 4th run, respectively. Heterogeneous kinetic models are proposed for the reaction, and Langmuir–Hinshelwood model is found to be the appropriate one.

Compliance with ethical standards

Conflicts of interest The authors declare that they have no conflicts of interest.

References

1. Ali MA, Siddiki SMAH, Onodera W et al (2015) Amidation of carboxylic acids with amines by Nb_2O_5 as a reusable Lewis acid catalyst. ChemCatChem 7:3555–3561. https://doi.org/10.1002/cctc.201500672

2. Ballini R, Bosica G, Carloni S et al (1998) Zeolite HSZ-360 as a new reusable catalyst for the direct acetylation of alcohols and phenols under solventless conditions. Tetrahedron Lett 39:6049–6052. https://doi.org/10.1016/S0040-4039(98)01244-1

3. Nishiguchi T, Kawamine K, Ohtsuka T (1992) Highly selective monoacylation of symmetric diols catalyzed by metal sulfates supported on silica gel. J Org Chem 57:312–316. https://doi.org/10.1021/jo00027a054

4. Iqbal J, Srivastava RR (1992) Cobalt(II) chloride catalyzed acylation of alcohols with acetic anhydride: Scope and mechanism. J Org Chem 57:2001–2007. https://doi.org/10.1021/jo00033a020

5. Saravanan P, Singh VK (1999) An efficient method for acylation reactions. Tetrahedron Lett 40:2611–2614. https://doi.org/10.1016/S0040-4039(99)00229-4

6. Alleti R, Perambuduru M, Samantha S, Reddy VP (2005) Gadolinium triflate: an efficient and convenient catalyst for acetylation of alcohols and amines. J Mol Catal A Chem 226:57–59. https://doi.org/10.1016/j.molcata.2004.09.024

7. Alleti R, Woon SO, Perambuduru M et al (2005) Gadolinium triflate immobilized in imidazolium based ionic liquids: a recyclable catalyst and green solvent for acetylation of alcohols and amines. Green Chem 7:203–206. https://doi.org/10.1039/b416359a

8. Izumi J, Shiina I, Mukaiyama T (1995) An efficient esterification reaction between equimolar amounts of free carboxylic acids and alcohols by the combined use of octamethylcyclotetrasiloxane and a catalytic amount of titanium(iv) chloride tris(trifluoromethanesulfonate). Chem Lett 24:141–142

9. Kumar AK, Chattopadhyay TK (1987) Catalytic role of diorganotin dichloride in esterification of carboxylic acids. Tetrahedron Lett 28:3713–3714. https://doi.org/10.3390/ma9070557

10. Likhar PR, Arunndhathi R, Ghosh S, Kantam ML (2009) Polyaniline nanofiber supported $FeCl_3$: an efficient and reusable heterogeneous catalyst for the acylation of alcohols and amines with acetic acid. J Mol Catal A Chem 302:142–149. https://doi.org/10.1016/j.molcata.2008.12.011

11. Chowdhury AH, Ghosh S, Islam SM (2018) Flower-like AgNPs@m-MgO as an excellent catalyst for CO_2 fixation and acylation reactions under ambient conditions. New J Chem 42:14194–14202. https://doi.org/10.1039/c8nj02286k

12. Mandi U, Roy AS, Banerjee B, Islam SM (2014) A novel silver nanoparticle embedded mesoporous polyaniline (mPANI/Ag) nanocomposite as a recyclable catalyst in the acylation of amines and alcohols under solvent free conditions. RSC Adv 4:42670–42681. https://doi.org/10.1039/c4ra06182a

13. Sreedhar B, Arunndhathi R, Reddy MA, Parthasarathy G (2009) Highly efficient heterogenous catalyst for acylation of alcohols and amines using natural ferrous chamosite. Appl Clay Sci 43:425–434. https://doi.org/10.1016/j.clay.2008.10.001

14. Choudary BM, Bhaskar V, Kantam ML et al (2001) Acylation of amines with carboxylic acids: the atom economic protocol catalysed by Fe(III)-montmorillonite. Catal Lett 74:207–211. https://doi.org/10.1023/A:1016662015856

15. Choudhary VR, Jana SK, Patil NS (2001) Acylation of benzene over clay and mesoporous Si-MCM-41 supported InCl₃, $GaCl_3$ and $ZnCl_2$ catalysts. Catal Lett 76:235–239. https://doi.org/10.1023/A:1012313726908

16. Skjak-Braek G, Grasdalen H (1989) Inhomogeneous polysaccharide ionic gels. Carbohydr Polym 10:31–54. https://doi.org/10.1016/0144-8617(89)90030-1

17. Rees DA, Welsh EJ (1977) Secondary and tertiary structure of polysaccharides in solutions and gels. Angew Chemie Int Ed English 16:214–224. https://doi.org/10.1002/anie.197702141

18. Rees DA (1981) Polysaccharide shapes and their interactions—some recent advances. Interactions 53:1–14. https://doi.org/10.1351/pac198153010001

19. Utech S, Boccaccini AR (2016) A review of hydrogel-based composites for biomedical applications: enhancement of hydrogel properties by addition of rigid inorganic fillers. Springer, New York

20. Liu J, Zhou H, Wang Q et al (2012) Reduced graphene oxide supported palladium-silver bimetallic nanoparticles for ethanol electro-oxidation in alkaline media. J Mater Sci 47:2188–2194. https://doi.org/10.1007/s10853-011-6022-6

21. Zhang H, Peng M, Cheng T et al (2018) Silver nanoparticles-doped collagen–alginate antimicrobial biocomposite as potential wound dressing. J Mater Sci 53:14944–14952. https://doi.org/10.1007/s10853-018-2710-9

22. Liang M, Zhang G, Feng Y et al (2018) Facile synthesis of silver nanoparticles on amino-modified cellulose paper and their catalytic properties. J Mater Sci 53:1568–1579. https://doi.org/10.1007/s10853-017-1610-8

23. Simon T, Wu CS, Liang JC et al (2016) Facile synthesis of a biocompatible silver nanoparticle derived tripeptide supramolecular hydrogel for antibacterial wound dressings. New J Chem 40:2036–2043. https://doi.org/10.1039/c5nj01981h

24. Supriya, Basu JK, Sengupta S (2019) Catalytic reduction of nitrobenzene using silver nanoparticles embedded calcium alginate film. J Nanosci Nanotechnol 19:7487–7492. https://doi.org/10.1166/jnn.2019.16669

25. Li WR, Xie XB, Shi QS et al (2010) Antibacterial activity and mechanism of silver nanoparticles on *Escherichia coli*. Appl Microbiol Biotechnol 85:1115–1122. https://doi.org/10.1007/s00253-009-2159-5

26. Liu J, Li X, Zeng X (2010) Silver nanoparticles prepared by chemical reduction-protection method, and their application in electrically conductive silver nanopaste. J Alloys Compd 494:84–87. https://doi.org/10.1016/j.jallcom.2010.01.079

27. Kim KD, Han DN, Kim HT (2004) Optimization of experimental conditions based on the Taguchi robust design for the formation of nano-sized silver particles by chemical reduction method. Chem Eng J 104:55–61. https://doi.org/10.1016/j.cej.2004.08.003

28. Shinde VV, Jadhav PR, Kim JH, Patil PS (2013) One-step synthesis and characterization of anisotropic silver nanoparticles: application for enhanced antibacterial activity of natural fabric. J Mater Sci 48:8393–8401. https://doi.org/10.1007/s10853-013-7651-8

29. Saha S, Pal A, Kundu S et al (2010) Photochemical green synthesis of calcium-alginate-stabilized Ag and Au nanoparticles and their catalytic application to 4-nitrophenol reduction. Langmuir 26:2885–2893. https://doi.org/10.1021/la902950x

30. Lin S, Huang R, Cheng Y et al (2013) Silver nanoparticle-alginate composite beads for point-of-use drinking water disinfection. Water Res 47:3959–3965. https://doi.org/10.1016/j.watres.2012.09.005

31. Asthana A, Verma R, Singh AK et al (2016) Silver nanoparticle entrapped calcium-alginate beads for Fe(II) removal via adsorption. Macromol Symp 366:42–51. https://doi.org/10.1002/masy.201650045

32. Liu Y, Zhao JC, Zhang CJ et al (2015) Bio-based nickel alginate and copper alginate films with excellent flame retardancy: Preparation, flammability and thermal degradation behavior. RSC Adv 5:64125–64137. https://doi.org/10.1039/c5ra11048c

33. Alemdar N (2016) Fabrication of a novel bone ash-reinforced gelatin/alginate/hyaluronic acid composite film for controlled drug delivery. Carbohydr Polym 151:1019–1026. https://doi.org/10.1016/j.carbpol.2016.06.033

34. Yang N, Wang R, Rao P et al (2019) The fabrication of calcium alginate beads as a green sorbent for selective recovery of Cu(II) from metal mixtures. Crystals 9:255. https://doi.org/10.3390/cryst9050255

35. Rowbotham JS, Dyer PW, Greenwell HC et al (2013) Copper(II)-mediated thermolysis of alginates: a model kinetic study on the influence of metal ions in the thermochemical processing of macroalgae. Interface Focus. https://doi.org/10.1098/rsfs.2012.0046

36. Torres E, Mata YN, Blázquezy ML et al (2005) Gold and silver uptake and nanoprecipitation on calcium alginate beads. Langmuir 21:7951–7958. https://doi.org/10.1021/la046852k

37. Kora AJ, Sashidhar RB, Arunachalam J (2010) Gum kondagogu (Cochlospermum gossypium): a template for the green synthesis and stabilization of silver nanoparticles with antibacterial application. Carbohydr Polym 82:670–679. https://doi.org/10.1016/j.carbpol.2010.05.034

38. Zhao X, Xia Y, Li Q et al (2014) Microwave-assisted synthesis of silver nanoparticles using sodium alginate and their antibacterial activity. Colloids Surf A Physicochem Eng Asp 444:180–188. https://doi.org/10.1016/j.colsurfa.2013.12.008

39. Wang CY, Huang KS, Yang CH et al (2014) A facile synthesis of gold nanoparticles-alginate composite spheres. Int J Latest Res Sci Technol 3:139–143

40. Grosjean R, Delacroix S, Gouget G et al (2015) Production of ultra-high concentration calcium alginate beads with prolonged dissolution profile. RSC Adv 5:36687–36695. https://doi.org/10.1039/C5RA03862F

41. Amirmoghadam H, Sadr MH, Aghabozorg H et al (2018) The effect of molybdenum on the characteristics and catalytic properties of $M/Cs_{1.5}H_{1.5}PW_{12}O_{40}/Al_2O_3$ (M = Ni or/and Mo) nanocatalysts in the hydrocracking of n-decane. React Kinet Mech Catal 125:983–994. https://doi.org/10.1007/s11144-018-1456-3

42. Bhadra KH, Yadav GD (2018) Solventless triarylmethane synthesis via hydroxyalkylation of anisole with benzaldehyde by modified heteropoly acid on mesocellular foam silica (MCF). Mol Catal 455:150–158. https://doi.org/10.1016/j.mcat.2018.06.003

43. Waghmode SB, Thakur VV, Sudalai A, Sivasanker S (2001) Efficient liquid phase acylation of alcohols over basic ETS-10 molecular sieves. Tetrahedron Lett 42:3145–3147. https://doi.org/10.1016/S0040-4039(01)00389-6